ISSN (Print) 1226-1750
ISSN (Online) 2233-6656
Journal of Magnetics 27(2), 210-216 (2022) https://doi.org/10.4283/JMAG.2022.27.2.210

Performance Evaluation of MRI Based on Newly Developed MRiLab Simulation Using Inversion Recovery Pulse Sequence with Various Inversion Times

Gaeun Baek, Jun Lim, Jihyun Yoon, and Youngjin Lee*

Department of Radiological Science, Gachon University, 191, Hambakmoero, Yeonsu-gu, Incheon, Republic of Korea

(Received 11 April 2022, Received in final form 27 May 2022, Accepted 13 June 2022)

Among the representative types of magnetic resonance imaging (MRI) sequences, inversion recovery (IR) can improve the ability to detect brain lesions. The purpose of this study was to confirm the MRI characteristics according to TI changes in IR sequences. In this study, the MRiLab simulation program-a newly developed, well-validated program-was used to quantitatively analyze image characteristics with respect to the TI value in the IR sequence. Brain tissue phantom and standard phantom images were acquired by changing the TI at 100-ms intervals from 100 to 2,500 ms. In brain tissue phantom images, signal intensity (SI) values showed the lowest signals at TI values of 400, 700, and 2,500 ms in the white matter (WM), gray matter (GM), and cerebrospinal fluid (CSF), respectively. The contrast evaluated in CSF-WM was superior at 400 ms and the lowest at 1,800 ms. In addition, the contrast evaluated in WM-GM was superior at 400 ms and the lowest at 1,500 ms. In the case of the brain standard phantom, the SI and contrast showed the same tendency as brain tissue phantom. In conclusion, an appropriate TI value was derived for obtaining images with excellent SI and contrast between brain tissues using a newly developed simulation program.

Keywords : Magnetic resonance imaging (MRI), Inversion recovery (IR), Inversion time (TI), MRiLab simulation program, quantitative evaluation of image quality

1. Introduction

Magnetic resonance imaging (MRI) is a diagnostic technique that utilizes a series of phenomena in which protons placed in a static field are excited and relaxed according to their absorption of electromagnetic waves [1]. MRI uses magnetic fields and nonionizing radiation; therefore, unlike other radiographic devices, it is non-invasive and does not involve exposure to radiation, and there is little risk from scanning [2]. In addition, it provides a high contrast for soft tissues and good resolution due to its excellent signal-to-noise ratio. It provides useful morphological and functional information for diagnosis as it can acquire multidirectional images in the sagittal, coronal, and transverse planes without changing the patient's position during the examination [3]. According to reports on imaging diagnosis, MRI showed excellent accuracy at 93 % compared with computed tomography, which was 87 % accurate in the identification and differential diagnosis of lesions. Moreover, the usefulness of MRI had been proved [4, 5].

In general, in addition to spin echo (SE) techniques but several sequences with excellent lesion detection efficiency are used in MRI because parameters must be adjusted to detect lesions, thereby resulting in excellent lesion detection efficiency [6]. These sequences include gradient echo adjusting the flip angle, fast spin echo adjusting the echo train length, and inversion recovery (IR) adjusting the inversion time (TI) [7-9].

The IR sequence is used to effectively detect lesions by maximizing the T1 contrast between tissues [10]. This sequence stimulates the 180° radiofrequency (RF) pulse prior to the 90° RF pulse in a typical SE sequence. After inverting the longitudinal magnetization, images are obtained by applying the existing 90° and 180° RF pulses [11]. The delay time between the leading 180° RF pulse inversion wave and 90° RF pulse excitation wave in the IR sequence is called the TI. The length of the TI has led to the development of a short tau inversion recovery (STIR) technique, which removes fat signals using short TI, and a fluid-attenuated inversion recovery (FLAIR) technique that removes the signal of a liquid component

*Corresponding author: Tel: +82-32-820-4362
Fax: +82-32-822-4449, e-mail: yj20@gachon.ac.kr

using a long TI. Compared with T1-weighted and T2-weighted images, STIR imaging is known to be effective in diagnosing fibrofatty lesions. FLAIR imaging enables the detection of lesions around the cerebrospinal fluid (CSF) in a conventional T2-weighted image [12, 13]. As such, because a difference occurs in the signal and contrast of each tissue in the image according to the length of the TI, the detection of the lesion can be facilitated due to this difference [14].

Increasing interest in the computer-assisted, quantitative analysis of medical image data has led to the development of well-validated programs. With these programs, it is possible to perform various simulations without directly testing patients in clinics. As a representative program, the BrainWeb simulation program can perform MRI simulations using random values of pulse sequences, source digital phantoms, and collection artifacts, and several studies have been conducted on MR images using this program [15-19]. In addition, research has been carried out using the MRiLab simulation program, which is a simulation program that can conduct virtual MR experiments on the brain and has a high degree of consistency with the actual brain with a simple operation that can easily adjust various MR image acquisition parameters [20]. Compared with other simulation programs, MRiLab simulation program can use much more various sequences, phantoms and parameters. In addition, the coil, sequence, RF pulse, motion, etc. can be designed within the program, and if necessary, various types of noise can be added and quantitative evaluation can be performed. However, despite these advantages of this simulation program, few MRI studies have been conducted with MRiLab. Therefore, our research team performed a study to determine the optimal values by adjusting the MRI parameters–flip angle, number of excitations, and bandwidth–in the MRiLab simulation program, and confirmed the reliability of the program [21].

Based on this reliability, the purpose of this study was to confirm the MRI characteristics according to TI changes IR sequences using the MRiLab simulation program. For this study, brain tissue phantom and brain standard phantom images were obtained using the MRiLab simulation program, followed by quantitative evaluation of signal intensity (SI) and contrast to analyze the results.

2. Materials and Methods

2.1. MRiLab simulation program

The MRiLab simulation program version 13 used in this study was modeled by Madison's University of Wisconsin based on a system similar to an actual MRI device (GE Discovery MR750, GE Healthcare, USA). This program can simulate MR signal formation, k-space acquisition, and MR image reconstruction. Thus, an image can be obtained by designing an MR sequence and configuring various coils. In addition, MRiLab was used in this study because it was possible to adjust the variables with simple manipulation and acquire images within a short period [20]. Because only brain images can be acquired through the MRiLab simulation program, brain tissue phantoms that represent signals from brain tissues, such as the white matter (WM), gray matter (GM), and CSF, were used in this study. After acquiring brain tissue phantom images according to TI changes in the IR sequence, the images of brain standard phantoms were obtained under the same conditions and quantitative evaluation was performed.

2.2. Parameters for acquiring IR sequence images

After fixing all variables such as repetition time, echo time, and noise level in the IR sequence of the MRiLab simulation program, only TI was changed from 100 to 2,500 ms at 100 ms intervals to acquire the brain tissue phantom (WM/GM/CSF) and brain standard phantom images. Table 1 shows the parameter values of the MRiLab simulation program used for image acquisition.

2.3. Quantitative evaluation

To quantitatively evaluate the images obtained through the MATLAB program, the regions of interest (ROIs) of the WM, GM, and CSF in brain tissue phantom and brain standard phantom images were set as shown in Fig. 1. In Fig. 1, ROI_{CSF} 1 represents the ROI in the CSF, ROI_{WM} represents the ROI in the WM, and ROI_{GM} represents the ROI in the GM. Figs. 1(a) and (b) are examples of images obtained using the brain tissue phantom and brain standard phantom, respectively. The SI and contrast of the acquired images were measured to analyze the characteristics of the images, and the equations (1) and (2) were used to determine the contrast [22]:

Table 1. Parameters for acquiring magnetic resonance images with the MRiLab simulation program

Sequence	Inversion time (ms)	TR (ms)	TE (ms)	Noise level (%)
Inversion recovery	From 100 to 2,500 ms at 100 ms intervals	15,000	50	0

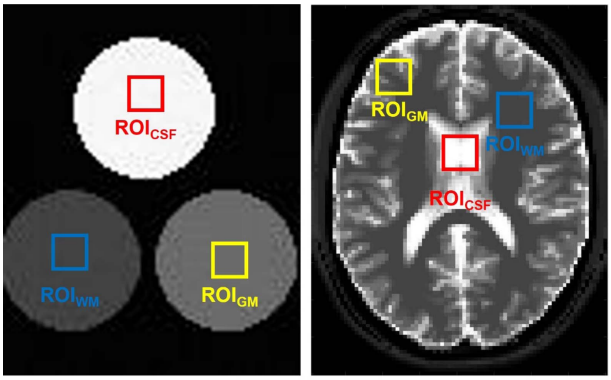

Fig. 1. (Color online) Setting of the region of the interest in the acquired (a) brain tissue phantom (WM/GM/CSF) and (b) brain standard phantom image

$$SI = \frac{S_T}{N} \tag{1}$$

where S_T refers to the sum of all the pixels in the ROI, and N refers to the number of pixels in the ROI.

$$Contrast = |S_A - S_B| \tag{2}$$

where S_A is the average SI value in the target tissue region and S_B is the average SI value in the background tissue region.

3. Results

In this study, the characteristics of each tissue were quantitatively evaluated according to the TI change in the IR sequence, using the brain tissue phantom (WM/GM/CSF) and brain standard phantom through the MRiLab simulation program.

3.1. Brain tissue phantom (WM/GM/CSF) images and quantitative evaluation results

Figure 2 shows images acquired from 100 to 2,500 ms by changing only the TI at 100 ms intervals after fixing all the parameters in the brain tissue phantom. Fig. 3 shows a graph of the SI results of the WM, GM, and CSF based on the acquired images. As a result of analyzing the SI graph of each tissue, the WM showed the lowest signal at TI 400 ms, which increased to TI 1,700 ms. The GM showed the lowest signal at TI 700 ms, which and

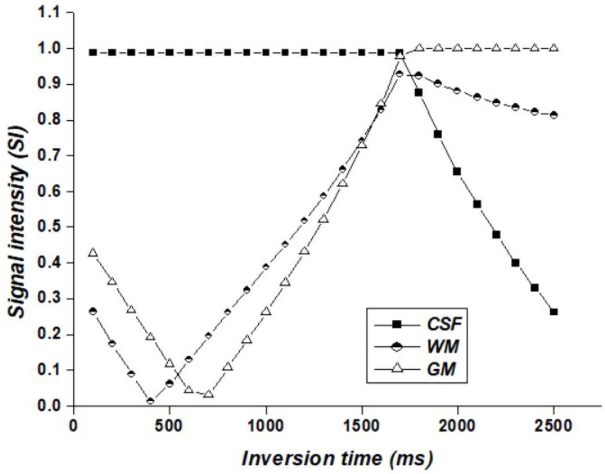

Fig. 3. Signal intensity of each tissue in brain tissue phantom (WM/GM/CSF) images acquired by changing the inversion time.

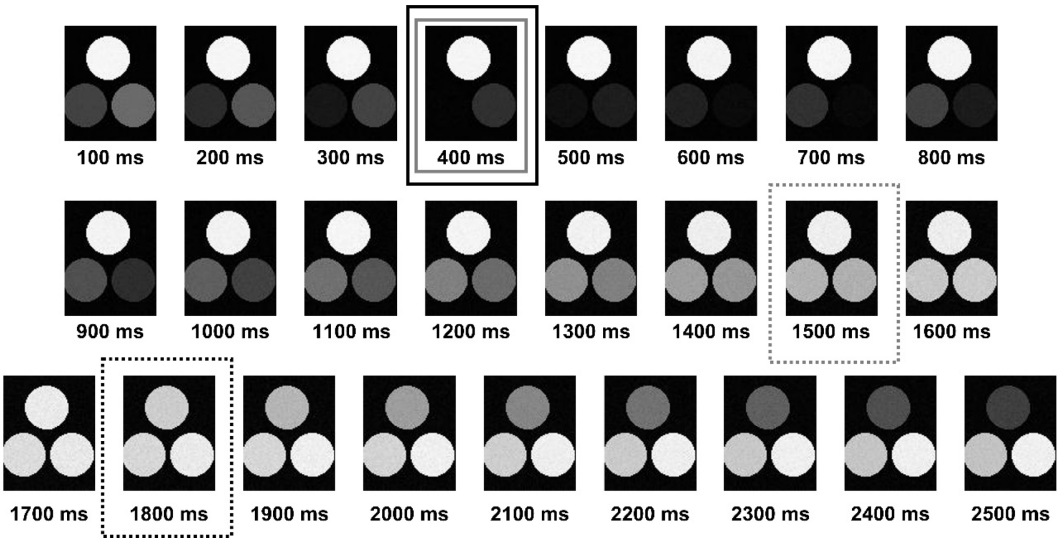

Fig. 2. Brain tissue phantom (WM/GM/CSF) images acquired by changing the inversion time using the MRiLab simulation program.

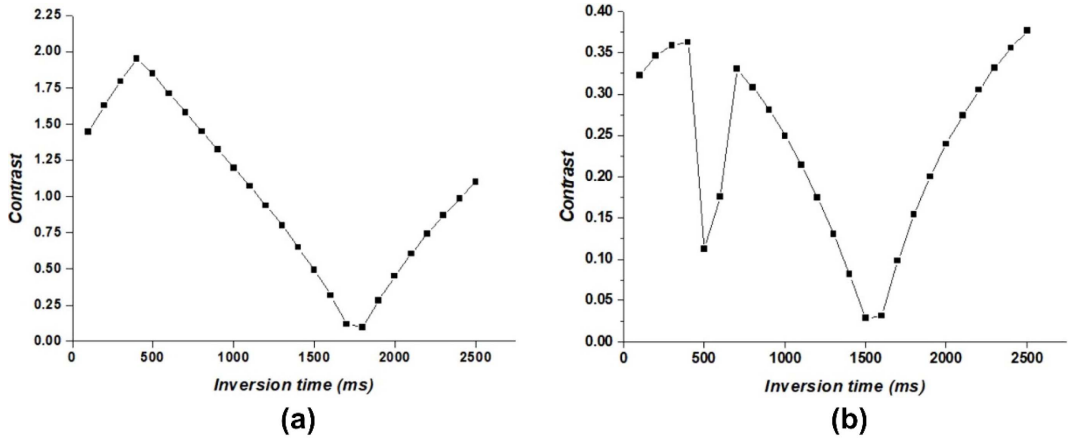

Fig. 4. Contrast of each tissue in brain tissue phantom (WM/GM/CSF) images acquired by changing the inversion time: (a) CSF-WM contrast and (b) WM-GM contrast.

increased to TI 2,500 ms. The CSF maintained a constant signal until TI 1,700 ms but decreased after TI 1,800 ms. Figs. 4(a) and (b) show the contrast in CSF-WM and WM-GM, respectively, in the brain tissue phantom according to the TI value. The CSF-WM contrast was the best at TI 400 ms, and the WM-GM contrast was superior at TI of 400 and 2,500 ms. The GM-CSF contrast was not shown because the GM and CSF tissues were not adjacent to each other on the brain MR and, therefore, difficult to compare.

3.2. Brain standard phantom images and quantitative evaluation

Figure 5 shows images acquired from 100 to 2,500 ms by changing only the TI at 100-ms intervals after fixing all the parameters in the brain standard phantom. Fig. 6

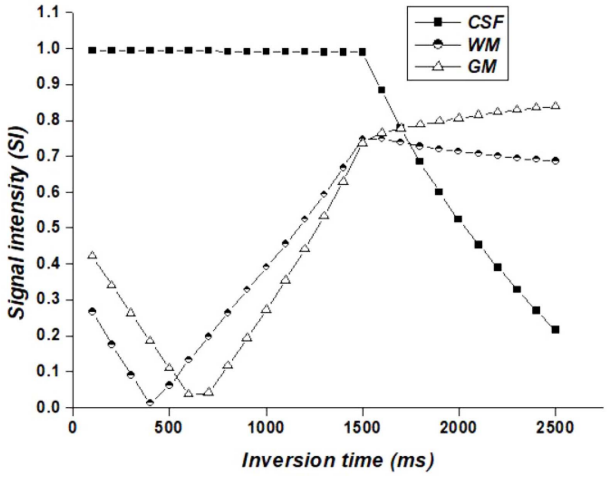

Fig. 6. Signal intensity of each tissue in brain standard phantom images acquired by changing the inversion time.

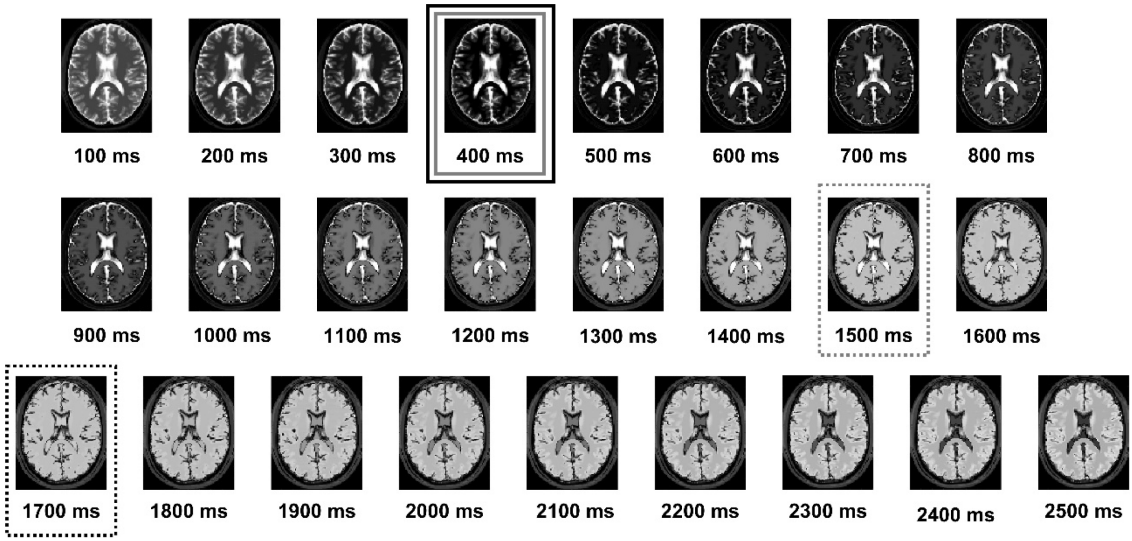

Fig. 5. Brain standard phantom images acquired by changing the inversion time using the MRiLab simulation program.

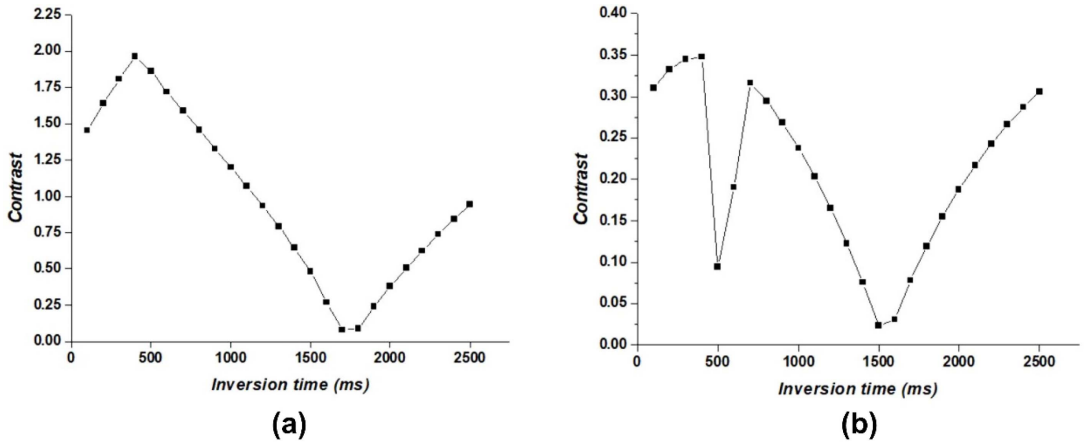

Fig. 7. Contrast of each tissue in brain standard phantom images acquired by changing the inversion time: (a) Cerebrospinal fluid-white matter (WM) contrast and (b) WM-gray matter contrast.

shows a graph of the SI results of the WM, GM, and CSF in the brain standard phantom images acquired by changing TI. The analysis of the SI graph of each tissue showed, the lowest signals for WM, GM, and CSF at 400, 700, and 2,500 ms, respectively. Figs. 7(a) and (b) show graphs for contrast in the CSF-WM and WM-GM, respectively, for the brain standard phantom according to the TI value. According to the graph, the CSF-WM contrast showed the largest difference at TI 400 ms and the smallest difference at 1,800 ms. The WM-GM contrast also showed the largest difference at TI 400 ms, but the smallest difference at 1,500 ms.

4. Discussion

The signal of the tissue changes as the length of TI changes in the IR sequence, and these can make meaningful differences like the contrast between tissues and resolution. Thus, through these meaningful differences, the detection of the lesion can be facilitated. Therefore, in this study, the SI and contrast changes in the WM, GM, and CSF were quantitatively evaluated when TI was changed from 100 to 2,500 ms at 100-ms intervals in the brain tissue phantom image. Subsequently, the SI and contrast changes of the WM, GM, and CSF were quantitatively evaluated in the brain standard phantom images under the same conditions and the results were compared.

In Fig. 2, the black solid line is the brain tissue phantom image at the TI with the best CSF-WM contrast, while the black dotted line represents the image at the TI with the lowest CSF-WM contrast. The gray solid line represents the brain tissue phantom image at the TI with the best WM-GM contrast, the gray dotted line represents the image at the lowest TI. As the difference in CSF-WM contrast was the largest at TI of 400 ms, the CSF was clearly visible, and the tissue could be distinguished. In the graph in Fig. 4(a), the contrast difference between the two tissues was the largest at 400 ms. However, although both the WM and CSF showed high SI at TI 1,800 ms, the contrast was the lowest, making it difficult to distinguish between the tissues. However, the CSF-WM contrast increased after 1,800 ms, enhancing the differentiation of WM at 2,500 ms. If we examine the WM-GM contrast for the TI indicated by gray lines, we see that the SI of the WM showed the lowest value at TI 400 ms, while the SI of GM showed the lowest value at TI 700 ms. Accordingly, the WM-GM contrast difference was the largest for the corresponding TI, facilitating the detection of GM at TI 400 ms and of WM at 700 ms. However, although both WM and GM tissues showed a high SI at a TI of 1,500 ms, it was difficult to distinguish between the tissues because the contrast difference was the lowest.

To confirm this tendency, a brain standard phantom was acquired under the same conditions and compared with the brain tissue phantom. The tissue changes in the two phantoms showed the same tendency. In Fig. 5, the black solid line is the brain standard phantom image at the TI with the best CSF-WM contrast, while the black dotted line represents the image at the TI with the lowest CSF-WM contrast. The gray solid line is the image at the TI with excellent WM-GM contrast, while the gray dotted line represents the image at the TI with the lowest WM-GM contrast. Similar to the brain tissue phantom, the SI of the WM showed the lowest signal, whereas the CSF-WM contrast difference was the largest at a TI of 400 ms; therefore, this condition was the best for the identification of CSF. As the SI of the CSF had the lowest signal at a TI 2,500 ms, it was easy to confirm the WM. Unlike the

brain tissue phantom that showed the lowest CSF-WM contrast at TI 1,800 ms, the contrast difference was the lowest at 1,700 ms in the brain standard phantom. It is believed that this difference occurred because the types of phantoms used were different. Comparing the WM-GM contrast in the gray box in Fig. 5 showed that, the SI of the WM was the lowest at TI 400 ms, as in the brain tissue phantom, making it easy to identify the GM. At TI 600 ms, the SI of the GM showed the lowest value, and it was easy to identify the WM. At TI 1,500 ms, both WM and GM tissues showed high SI, but because the difference in contrast was the smallest, it was difficult to distinguish between the tissues. By quantitatively comparing the brain tissue phantom and the brain standard phantom, it was confirmed that the tendency of each tissue was consistent according to the TI change in the two phantoms.

According to the SI change graph, the WM, GM, and CSF in the brain tissue phantom showed the lowest signals at 400, 700, and 2,500 ms, respectively. Similarly, the SI of the WM, GM, and CSF in the brain standard phantom showed the lowest signals at TI 400, 700, and 2,500 ms, and the tendency of the SI change graph was consistent.

According to the contrast change graph, the CSF-WM contrast of the brain tissue phantom was the highest at TI 400 ms and the lowest at 1,800 ms. The WM-GM contrast was the highest at TI 400 ms and the lowest at 1,500 ms. Similarly, the TI with the best CSF-WM contrast of the brain standard phantom was 400 ms, and the lowest TI was 1,700 ms. Although there was a slight difference from the brain tissue phantom, the overall tendency was similar. The WM-GM contrast of the brain standard phantom was also the best at a TI of approximately 400 ms and the lowest at a TI of 1,500 ms, similar to the contrast in the brain tissue phantom.

Both brain tissue phantom and brain standard phantom showed different results from previous studies, which are evident in the SI of the WM. In clinical studies on tissue SI changes according to TI changes, the SI of the WM showed the lowest signal at TI 400 ms and continued to increase as TI increased [23-25]. In contrast, the SI of the WM decreased slightly after TI 1,700 ms, but the overall tendency for SI of the WM was consistent with previous studies. In addition, although the MRiLab simulation program was designed based on the real device, this study was conducted only by the simulation data. Therefore, to overcome these limitations, we intend to conduct further simulation and an actual experiment in the future, and check whether similar results are obtained. In addition, not only using the MRiLab simulation program, we intend to improve an accuracy of our results by using the data acquired from validated program such as BrainWeb simulation program.

In this study, two types of phantom images were acquired by changing only the TI after fixing all parameters using the well-validated MRiLab simulation program. This again proved the reliability of the program. In addition, when acquiring MRI brain IR images, our results are expected to be used as basic data to set an appropriate TI in acquiring images with excellent contrast for each tissue.

5. Conclusion

In this study, it was confirmed that the WM, GM, and CSF on MR images changed according to the change in TI in the IR sequence. As a result, in the brain tissue phantom images, the SI was the lowest at TI 400 ms for WM, 700 ms for GM, and 2,500 ms for CSF. The same trend was observed in the brain standard phantom. The CSF-WM contrast of the brain tissue phantom was the best at TI 400 ms and the lowest at approximately 1,800 ms. The CSF-WM contrast of the brain standard phantom was also the best at a TI of 400 ms and lowest at 1,700 ms. The WM-GM contrast was the best at TI 400 ms for both the brain tissue phantom and brain standard phantom and was the lowest at 1,500 ms. At the TI corresponding to the lowest CSF-WM contrast, there was a slight difference between the two phantoms, but it was confirmed that the CSF-WM contrast results in both phantoms showed the same overall tendency. As a result, the SI and contrast of each tissue could be evaluated according to the TI length, and the optimal TI useful for observing the target tissue was identified. Thus, this study provides optimal TI for different brain tissues that will be useful for applying to MR images obtained with the IR sequence using a newly developed well-validated program, MRiLab simulation program.

References

[1] A. Berger, BMJ: British Medical Journal **324**, 35 (2002).
[2] D. Formica and S. Silvestri, BioMedical Engineering OnLine **3**, (2004). https://doi.org/10.1186/1475-925X-3-11
[3] R. T. Constable and R. M. Henkelman, Journal of Computer Assisted Tomography **15**, 297 (1991).
[4] M. Trede, B. Rumstadt, K. Wendl, J. Gaa, K. Tesdal, K. J. Lehmann, H. J. Meier-Willersen, P. Pescatore, and J. Schmoll, Annals of Surgery **226**, 393 (1997).
[5] M. Takahashi, H. Uematsu, and H. Hatabu, European Journal of Radiology **46**, 45 (2003).
[6] M. H. Jiang, C. He, J. M. Feng, Z. H. Li, Z. Chen, F. H.

Yan, and Y. Lu, Scientific Reports **6**, (2016). doi: 10.1038/srep36995
[7] G. Walsh, T. Meagher, and C. Malamateniou, Radiography **27**, 561 (2021).
[8] S. Kim and J. D. Rhim, Journal of Magnetics **25**, 534 (2020).
[9] G. Sze, Y. Kawamura, C. Negishi, R. T. Constable, M. Merriam, K. Oshio, and F. Jolesz, Am. J. Neuroradiol. **14**, 1203 (1993).
[10] G. M. Bydder and I. R. Young, Journal of Computer Assisted Tomography **9**, 659 (1985).
[11] G. M. Bydder, J. V. Hajnal, and I. R. Young, Clinical Radiology **53**, 159 (1998).
[12] J. V. Hajnal, D. J. Bryant, L. Kasuboski, P. M. Pattany, B. D. Coene, P. D. Lewis, J. M. Pennock, A. Oatridge, I. R. Young, and G. M. Bydder, Journal of Computer Assisted Tomography **16**, 841 (1992).
[13] B. De Coene, J. V. Hajnal, P. Gatehouse, D. B. Longmore, S. J. White, A. Oatridge, J. M. Pennock, I. R. Young, and G. M. Bydder, Am. J. Neuroradiol. **13**, 1555 (1992).
[14] J. L. Bloem, M. Reijnierse, T. W. J. Huizinga, and A. H. M. van der Helm-van Mil, RMD Open **4**, (2018). doi:10.1136/rmdopen-2018-000728
[15] K. Doi, The British journal of radiology **78**, (2005). https://doi.org/10.1259/bjr/82933343
[16] R. K. S. Kwan, A. C. Evans, and G. B. Pike, IEEE Trans. Med. Imaging **18**, 1085 (1999).
[17] R. K. S. Kwan, A. C. Evans, and G. B. Pike, International Conference on Visualization in Biomedical Computing **1131**, 135 (1996).
[18] D. L. Collins, A. P. Zijdenbos, V. Kollokian, J. G. Sled, N. J. Kabani, C. J. Holmes, and A. C. Evans, IEEE Trans. Med. Imaging **17**, 463 (1998).
[19] Y. Wen, K. Xie, and L. He, Proceedings of the AAAI Conference on Artificial Intelligence **34**, 12452 (2020).
[20] F. Liu, J. V. Velikina, W. F. Block, R. Kijowski, and A. A. Samsonov, IEEE Trans. Med. Imaging **36**, 527 (2016).
[21] J. Lim, S. H. Kang, C. R. Park, and Y. Lee, J. Magn. **26**, 41 (2021).
[22] W. H. Choi, H. R. Choi,, E. Seo, J. Hwang, H. Oh, M. R. Kim, S. R. Han, M. S. Kin, S. H. Kang, and Y. Lee, Optik **183**, 241 (2019).
[23] S. A. Bobman, S. J. Riederer, J. N. Lee, T. Tasciyan, F. Farzaneh, and H. Z. Wang, Radiology **159**, 253 (1986).
[24] E. H. Middlebrooks, C. Lin, E. Westerhold, L. Okromelidze, P. Vibhute, S. S. Grewal, and V. Gupta, NeuroImage: Clinical **28**, (2020). https://doi.org/10.1016/j.nicl.2020.102449
[25] J. Wang, L. He, H. Zheng, and Z. L. Lu, PLOS ONE **9**, (2014). https://doi.org/10.1371/journal.pone.0096899